Reaction Chemistry & Engineering

ROYAL SOCIETY OF CHEMISTRY

PAPER

View Article Online
View Journal

Cite this: DOI: 10.1039/d5re00152h

Deactivation of Ni catalyst in three-phase CO_2 methanation

Mathias Held, * Anna Holfelder, Siegfried Bajohr and Thomas Kolb

Received 4th April 2025,
Accepted 6th August 2025

DOI: 10.1039/d5re00152h

rsc.li/reaction-engineering

In three-phase CO_2 methanation dibenzyl toluene is used as the liquid phase in a slurry bubble column reactor. At reactor temperatures (T_R) higher than 260 °C deactivation of the Ni/SiO_2 catalyst was observed. After deactivation for 120 h at T_R = 320 °C, stationary operation is possible with a loss of catalytic activity of ≈50%. Based on experimental results, it can be stated that deactivation is caused by decomposition of dibenzyl toluene at high reactor temperature, resulting in carbon deposition on the catalyst surface.

1 Introduction

In future energy systems, the share of renewable electrical energy from regenerative sources like wind and solar power will be high. Due to environmental influences such as daytime and weather, electrical energy production from these sources will be fluctuating, so processes for energy storage are needed to meet the demand.[1] Besides batteries or capacitors, power-to-gas technologies provide a possibility to store electrical energy from fluctuating sources. In this case, electrical energy is used to power electrolysis and produce hydrogen from water. The obtained hydrogen can be used directly or as a feedstock for downstream synthesis such as CO_2 methanation.[2] This route offers a high storage capacity using the natural gas grid.

In CO_2 methanation substitute natural gas is produced using H_2 from water electrolysis and CO_2 from ambient air and industrial or biological sources.[3,4] To allow the storage of renewable electrical energy various approaches address the transient operation of CO_2 methanation.[5–7] The main challenge regarding dynamic operation of the methanation reactor is heat management to avoid thermal deactivation of the catalyst.

One approach is three-phase CO_2 methanation: using the liquid phase dibenzyl toluene in a slurry bubble column reactor (SBCR), isothermal operation is possible even for high load changes.[8,9] The robustness regarding load and temperature changes in the SBCR allows dynamic operation of CO_2 methanation. In the SBCR a Ni/SiO_2 catalyst is used for CO_2 methanation. Lefebvre *et al.* determined reaction kinetics for the relevant operating conditions.[10] Sauerschell *et al.* showed robustness of the SBCR regarding dynamic operation of a 100 kW methanation pilot plant.[9]

Engler-Bunte-Insitut – Fuel Technology, Engler-Bunte-Ring 1, 76131 Karlsruhe, Germany. E-mail: mathias.held@kit.edu

For reactor design, it is crucial to address possible catalyst deactivation in chemical synthesis. There are numerous mechanisms that can lead to catalyst deactivation in CO_2 methanation. In three-phase CO_2 methanation additional deactivation mechanisms can occur due to the the liquid phase dibenzyl toluene (DBT, $C_{21}H_{20}$) present in the reactor. For example, the adsorption of DBT or decomposition of DBT which leads to adsorption of decomposition products or carbon deposition could decrease catalytic activity. On the other hand, deactivation mechanisms which are often observed in CO_2 methanation such as sintering can be avoided due to the good heat management in the reactor. For technical application, deactivation of the catalyst should be limited to avoid additional costs for catalyst regeneration or exchange. Therefore, reaction conditions that lead to catalyst deactivation have to be determined.

The goal of this work is to determine which reactor temperature leads to catalyst deactivation in three-phase CO_2 methanation, quantify the maximum loss of catalytic activity for steady-state operation and identify the underlying mechanisms responsible for catalyst deactivation.

To identify the mechanism relevant for catalyst deactivation an experimental exclusion approach is applied in this work: catalyst deactivation mechanisms in CO_2 methanation that are discussed in the literature are presented in section 2. Experiments are performed under different reaction conditions to rule out all mechanisms that are irrelevant. For evaluation of catalytic activity, CO_2 reaction rate is used and an experimental procedure is developed to account for DBT hydrogenation which occurs as a side reaction in three-phase CO_2 methanation.

2 Theory

2.1 Catalytic CO_2 methanation

CO_2 methanation was firstly described by Sabatier in 1902.[11] CO_2 and H_2 are converted to CH_4 and H_2O:

$$CO_2 + 4H_2 \rightleftharpoons CH_4 + 2H_2O \quad \Delta H_R = -165\ \text{kJ mol}^{-1} \qquad (1)$$

Different catalysts can be used (*e.g.* Ru, Fe and Rh). In industrial application Ni is often chosen, as it shows sufficient selectivity and activity for CO_2 methanation at a low price.[12,13] Reaction conditions range from T = 250–550 °C and p_{abs} = 1–100 bar.[14,15]

The reaction is highly exothermic so heat management is crucial for reactor design, especially for systems that have to cope with load changes.[16] Load changes are critical regarding thermal deactivation of the Ni catalyst used: an increase of the gas load (increased volume flow of educt gases) leads to more reaction heat being released at the catalyst surface. As a consequence, sintering of active sites on the catalyst surface is possible, which decreases catalyst activity.

In three-phase CO_2 methanation temperature hotspots are avoided even for high load changes and an almost isothermal operation is possible.[9] The reactor used is a slurry bubble column reactor (SBCR) shown in Fig. 1: catalyst particles are suspended in the liquid phase dibenzyl toluene and are fluidized by the entering gas flow. H_2 and CO_2 are evenly distributed at the bottom of the reactor using a gas sparger (*e.g.* a perforated plate). In the reactor, educt gases are dissolved in the liquid phases and converted to CH_4 and H_2O at the catalyst surface. The liquid phase DBT exhibits a high heat capacity and is present directly at the catalyst surface; therefore, reaction heat can be removed from the system without formation of temperature hotspots that are critical regarding thermal catalyst deactivation. In addition, the gas flow creates a high degree of mixing inside the reactor so isothermal operation is possible. The concept of using a slurry bubble column reactor for dynamically operated three-phase CO_2 methanation was validated on the 100 kW scale: Sauerschell *et al.*[9] employed a 100% gas load change during CO_2 methanation in a SBCR. The gas flow was ramped up within 30 s and a moderate rise of reactor temperature of 15 K was observed.

In summary, the introduction of liquid phase DBT in CO_2 methanation allows a highly dynamic operation which is of great interest regarding the load flexibility of chemical synthesis needed in future energy systems.

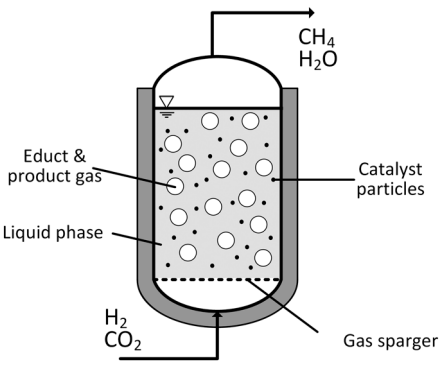

Fig. 1 Schematic drawing of a slurry bubble column reactor used for three-phase CO_2 methanation.

Possible catalyst deactivation mechanisms in three-phase CO_2 methanation. To determine the mechanisms which are relevant for catalyst deactivation in three-phase CO_2 methanation an experimental exclusion approach is applied. In the following section, catalyst deactivation mechanisms which are discussed in the literature for CO_2 methanation are presented. Exclusion of irrelevant mechanisms is performed by variation of reaction conditions in section 4.3.

There are many different mechanisms that can lead to catalyst deactivation in CO_2 methanation.[17,18] Bartholomew[19] divides catalyst deactivation mechanisms into three basic categories: thermal, mechanical and chemical deactivation.

Thermal catalyst deactivation mainly describes loss of active surface due to sintering or support interactions at high temperature.[19,20] To determine if a system is prone to thermal deactivation, the Hüttig temperature of the catalyst material can be determined.[21] For the experiments performed in this work, the maximum reactor temperature is limited to T_R = 320 °C. The Hüttig temperature ($T_{Hüttig}$) for the used Ni/SiO_2 catalyst is $T_{Hüttig}$ >450 °C for both active component and carrier, so thermal deactivation can be neglected.

Mechanical deactivation comprises loss of catalytic activity caused by attrition or crushing of catalyst particles as well as fouling on the catalyst surface.[19] Experiments presented in this work were performed in a continuous stirred-tank reactor (CSTR). Catalyst attrition is possible in both the SBCR and the CSTR because of the high shear forces present. However, for the experiments performed in the scope of this work mechanical deactivation caused by catalyst attrition is ruled out as a possible catalyst deactivation mechanism. At the reactor outlet a filter is installed which showed no catalyst particles even for experiments with long time on stream (280 h). Also, no catalyst discharge to the condensate vessel was observed.

Loss of catalytic surface caused by fouling is also possible in CO_2 methanation. One possibility is fouling by carbon deposition according to the Boudouard reaction:[22–24]

$$CO_2 + C \rightleftharpoons 2CO \quad \Delta H_R = -173\ \text{kJ mol}^{-1} \qquad (2)$$

Furthermore, methane pyrolysis could lead to carbon deposition. Both reactions are favored at high temperature and low H_2/CO ratio.[25,26] Carbon deposition is mainly discussed in CO methanation[27] but needs to be considered for CO_2 methanation as well since it is a combination of the reverse water gas shift reaction followed by CO methanation.[7]

Another possibility, which could be specifically relevant in three-phase methanation is carbon deposition by decomposition of dibenzyl toluene which is used as the liquid phase. This effect was already observed in dehydrogenation of dibenzyl toluene.[28–30] Decomposition of DBT was observed using Pt catalysts, with decomposition products benzyl toluene, benzene, toluene, xylene and methane. In this case, the catalyst was deactivated by carbon deposition on the catalyst surface which was formed in the decomposition reaction. Carbon deposition by decomposition

of higher hydrocarbons has also been discussed in methanation of biosyngas.[23]

Chemical deactivation mechanisms comprise the loss of catalytically active surface caused by side reactions of the active material or by catalyst poisoning. In this work a nickel catalyst is used for CO_2 methanation. For temperatures lower than 200 °C the formation of nickel tetracarbonyls is a possible side reaction:[22,31,32]

$$Ni_{(s)} + 4CO_{(g)} \rightleftharpoons Ni(CO)_{4(g)} \quad (3)$$

The reaction involves CO as a reactant but can also occur in CO_2 methanation in which the formation of CO is discussed as a reaction intermediate. The formation of nickel tetracarbonyls leads to gaseous discharge of Ni from the reactor or agglomeration of Ni particles in the case of direct decomposition.[22,31]

The second possibility for chemical deactivation is catalyst poisoning by adsorption of components on the catalyst surface.[19] These can be impurities in the educt gases, such as sulfuric components like H_2S or thiophenes.[24,33] In three-phase methanation impurities in the liquid phase DBT could also lead to chemical catalyst deactivation.

Furthermore, the adsorption of DBT on the catalyst surface needs to be considered. At a high degree of hydrogenation there are fewer aromatic DBT molecules that adsorb more strongly on the catalyst surface.[34] Thus, catalyst deactivation should be more pronounced at a low degree of hydrogenation if it is caused by DBT adsorption.

An additional effect that can cause the loss of catalytic activity is catalyst oxidation. This effect is not reported in CO_2 methanation but is observed in other three-phase systems such as Fischer–Tropsch synthesis.[35] For the sake of full consideration of possible deactivation mechanisms, catalyst oxidation is also addressed in this work.

For activation, the catalyst is reduced with H_2 according to eqn (4):

$$NiO_{(s)} + H_{2(g)} \rightleftharpoons Ni_{(s)} + H_2O_{(g)} \quad \Delta H_R = -2\ \text{kJ mol}^{-1} \quad (4)$$

In CO_2 methanation, H_2O is formed as a side product. This can lead to oxidation of the catalyst as the reverse reaction of eqn (4). In this case, NiO is formed, which is not active for CO_2 methanation.

2.2 DBT hydrogenation as a side reaction in three-phase CO_2 methanation

In three-phase CO_2 methanation DBT hydrogenation is observed as a side reaction competing for H_2.[36] The reaction is shown in eqn (5):

$$C_{21}H_{20} + 9H_2 \rightleftharpoons C_{21}H_{38} \quad \Delta H_R = -588\ \text{kJ mol}^{-1} \quad (5)$$

The extent of hydrogenation is described by the degree of hydrogenation (DoH). It describes the share of hydrogenated double bonds of DBT molecules in the evaluated sample according to eqn (6):

$$\text{DoH} = \frac{N_{\text{hydrogenated double bonds}}}{N_{\text{initial double bonds}}} \quad (6)$$

As DBT consists of three aromatic rings, hydrogenation of DBT is a stepwise reaction with the (intermediate) products H6-DBT (DoH = 1/3), H12-DBT (DoH = 2/3) and H18-DBT (DoH = 1). In the scope of the experiments presented in this work, DBT hydrogenation is operated in semi-batch mode. The reaction reduces the reaction rate of CO_2 methanation until chemical equilibrium of DBT hydrogenation is reached.[36] For a detailed analysis of catalyst deactivation in three-phase CO_2 methanation, the influence of DBT hydrogenation on the CO_2 reaction rate should be avoided. Therefore, the CO_2 reaction rate is evaluated when the DoH is constant, meaning the chemical equilibrium of DBT hydrogenation is reached (see experimental procedure in section 3.2.2).

3 Materials and methods

3.1 Experimental setup

CO_2 methanation and DBT hydrogenation experiments are performed in a continuous stirred-tank reactor (CSTR). Using this setup the influence of hydrodynamics and mass transport resistances can be neglected. This allows for direct evaluation of catalyst deactivation by comparison of reaction rates.

The absence of mass transport resistance was verified by variation of stirrer speed. Educt gas volume flow to the reactor is controlled using mass flow controllers. The temperature in the reactor is controlled using an electrical heating jacket. Product gases leave the reactor through an electrically heated pipe to avoid condensation of water and backflow to the reactor. The product gas flow is cooled in a condensate vessel, in which water and other evaporated components are collected. The composition of the remaining gas is then analyzed using an Agilent 490 Micro GC instrument.

For CO_2 methanation a commercially available NiO/SiO_2 catalyst is used. Before the start of the experiment the catalyst is activated by reduction with H_2. Catalyst reduction is performed in a fixed-bed reactor at T_R = 430 °C for t_{red} = 72 h. After activation, it is suspended in DBT in an inert atmosphere to avoid the oxidation of nickel. After transferring to the CSTR, the stirrer speed, reactor pressure and temperature are set. For pressure build-up, Ar is used as an inert gas. Once all reaction conditions are constant, the flow of educt gases is started. Throughout the experiment liquid samples are taken from the CSTR to determine the DoH of DBT.

To evaluate catalyst deactivation in three-phase CO_2 methanation, the catalytic activity needs to be determined from product gas composition. The catalyst which is used in this work exhibits high selectivity for CH_4,[37] hence side

reactions involving CO_2 are neglected and the CO_2 reaction rate r_{CO_2} is used to quantify the loss of catalytic activity:

$$r_{CO_2} = \frac{X_{CO_2}}{\tau_{mod,CO_2}} \quad (7)$$

CO_2 conversion X_{CO_2} is determined using the product gas composition measured by the micro GC and the volume flow set by the mass flow controllers:

$$X_{CO_2} = \frac{\dot{n}_{CO_2,in} - \dot{n}_{CO_2,out}}{\dot{n}_{CO_2,in}} \quad (8)$$

Further, the modified residence time of CO_2 is determined using the molar flow of CO_2 as well as catalyst mass:

$$\tau_{mod,CO_2} = \frac{m_{Cat}}{\dot{n}_{CO_2,in}} \quad (9)$$

The stoichiometric number S is used to characterize the educt gas flow in CO_2 methanation experiments. It describes the ratio of the molar flow of H_2 to the molar flow of CO_2 with their respective stoichiometric numbers according to eqn (1). S is 1 for a stoichiometric ratio of the molar flows.

$$S = \frac{\dot{n}_{H_2}}{4 \cdot \dot{n}_{CO_2}} \quad (10)$$

The DoH of DBT is determined by density measurement at T = 20 °C of liquid samples taken from the CSTR using a correlation for the specific isomeric mixture of DBT molecules used:[36]

$$DoH = 22.45 - 37.36 \cdot \left(\frac{\rho_{DBT}}{g\ cm^{-3}}\right) + 15.19 \cdot \left(\frac{\rho_{DBT}}{g\ cm^{-3}}\right)^2 \quad (11)$$

3.2 Evaluation of catalyst deactivation

3.2.1 Determination of reactor temperature that leads to catalyst deactivation. To determine the reactor temperature at which catalyst deactivation occurs, experiments at different reactor temperatures for a time on stream of 24 h are performed. For each experiment a new batch of DBT and fresh catalyst is used to ensure the same starting conditions. The experimental procedure is shown in Fig. 2.

Reactor pressure is set by dosing inert gas with the mass flow controllers, and reactor temperature is set using the electrical heating of the CSTR. Once reactor temperature and pressure are constant in the reactor, the flow of educt gases is continued for 24 h. To evaluate catalyst activity after 24 h the temperature is set to a reference temperature of T_{Ref} = 260 °C as preliminary experiments showed no catalyst deactivation at $T_R \leq 260$ °C. Therefore, this temperature was chosen as a reference to evaluate the catalytic activity by calculation of CO_2 reaction rate r_{CO_2} (see eqn (7)). If catalyst deactivation occurs, a lower r_{CO_2} should be observed at T_{Ref}. However, the calculated CO_2 reaction rates cannot be used to quantify catalyst deactivation since the chemical equilibrium of DBT hydrogenation is not reached at ToS = 24 h. Therefore, r_{CO_2} determined at T_{Ref} is influenced by the DBT hydrogenation reaction. The reactor pressure and molar flow of educt gases CO_2 and H_2 remain constant throughout the experiment.

3.2.2 Quantification of catalyst deactivation for steady-state operation using CO_2 reaction rate. To quantify the loss of catalytic activity for steady-state operation the CO_2 reaction rate r_{CO_2} is used (see eqn (7)). r_{CO_2} is influenced by DBT hydrogenation until chemical equilibrium is reached (DoH = const.). For the quantification of catalyst deactivation, the influence of DBT hydrogenation needs to be considered. Hence, the experimental procedure shown in Fig. 3 was chosen.

Reactor pressure is built up by dosing inert gas Ar using mass flow controllers; reactor temperature is set using the electrical heating of the CSTR. Once reactor temperature and pressure are constant, the flow of educt gases is started. At the start of the experiment a reactor temperature of T_R = 260 °C is set for ToS ≈ 120 h. This time period is chosen to allow DBT hydrogenation to reach its chemical equilibrium. Then, the reactor temperature is increased to T_R = 320 °C until steady-state operation regarding r_{CO_2} is reached. Once the CO_2 reaction rate stabilizes (up to ToS = 250 h), the reactor temperature is set again to T_{Ref} = 260 °C. The loss of catalytic activity is quantified by comparison of CO_2 reaction rate after operation at T_R = 320 °C (ToS = 227 h) with its value at

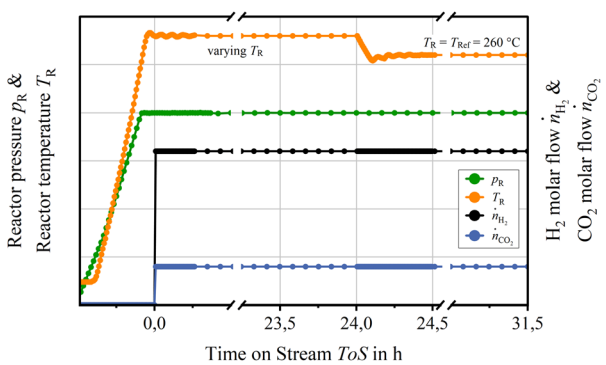

Fig. 2 Experimental procedure to determine reactor temperature that leads to catalyst deactivation.

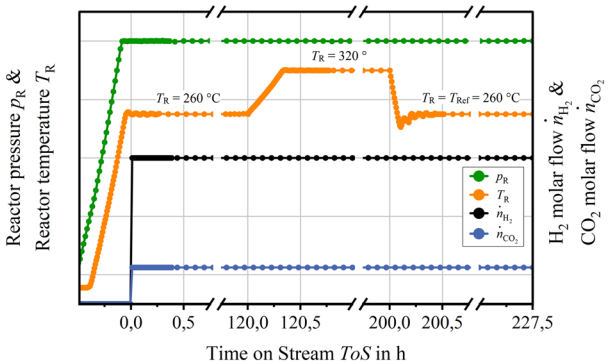

Fig. 3 Experimental procedure to quantify loss of catalytic activity for steady-state operation excluding the influence of DBT hydrogenation.

T_R = 260 °C after reaching the hydrogenation equilibrium (ToS = 120 h).

For the experiments aiming to identify the underlying catalyst deactivation mechanism a similar experimental procedure was chosen. Reaction conditions were adjusted to investigate the deactivation mechanisms discussed in section 2.1.

Apart from product gas analysis, the liquid phase and catalyst particle samples were analyzed to support the identification of the deactivation mechanism. Liquid phase samples were analyzed using a two-dimensional GC × GC to identify possible DBT decomposition products.

Samples of catalyst particles were analyzed using scanning electron microscopy (SEM) and thermogravimetric analysis (TGA) to check for residues on the catalyst surface.

4 Results

4.1 Determination of reactor temperature that leads to catalyst deactivation in three-phase CO_2 methanation

To determine the reactor temperature that leads to catalyst deactivation in three-phase CO_2 methanation, experiments were carried out according to the experimental procedure presented in section 3.2.1.

In Fig. 4 the CO_2 reaction rate r_{CO_2} (see eqn (7)) is shown under the same reaction conditions of T_{Ref} = 260 °C and p_{H_2} = 13.2 bar. These reaction conditions were set after the operating point: each experiment was conducted for ToS = 24 h at a specific reactor temperature T_R. During this ToS possible catalyst deactivation can occur. Comparison of the CO_2 reaction rates under the same conditions after ToS = 24 h allows the evaluation of the loss of catalytic activity dependent on reactor temperature. The CO_2 reaction rate is constant for T_R = 220–260 °C. For T_R >260 °C, a decrease in r_{CO_2} is observed. This can be explained by catalyst deactivation which occurs for T_R >260 °C. The loss of catalytic activity increases with T_R.

4.2 Quantification of catalyst deactivation for steady-state operation

To determine the reactor temperature that leads to catalyst deactivation a ToS of 24 h was chosen (see Fig. 4). However, after 24 h no steady-state operation of the reactor is reached, r_{CO_2} is still decreasing and DBT hydrogenation reaction has not reached chemical equilibrium. To quantify the loss in catalytic activity for steady-state operation, an experiment was carried out according to the experimental procedure presented in section 3.2.2. The CO_2 reaction rate r_{CO_2} observed is shown in Fig. 5.

At the start of the experiment, the reactor temperature was set to T_R = 260 °C for ToS ≈ 120 h. During this time hydrogenation of DBT occurs as a side reaction and reaches its chemical equilibrium, which can be seen by the rise in DoH and r_{CO_2}. T_R = 260 °C is chosen, because at this T_R no catalyst deactivation is observed (see Fig. 4). Once steady state regarding r_{CO_2} is reached, hydrogenation equilibrium is assumed. The temperature is then increased to provoke catalyst deactivation at T_R = 320 °C. The temperature increase leads to an increase of r_{CO_2} according to Arrhenius' law. However, the increase in r_{CO_2} is directly followed by a decrease within the first three hours of the operating point. Then a further but less pronounced decrease in r_{CO_2} is observed until steady state is reached after ToS ≈ 250 h.

The decrease of r_{CO_2} at T_R = 320 °C can be explained by catalyst deactivation. In the first three hours of the experiment, the loss in catalytic activity is high. This could be explained by deactivation caused by residues covering the catalyst surface. This film is most likely formed in the first hours in which deactivation occurs. In the following hours, film thickness is increasing, which leads to additional deactivation that is less pronounced.

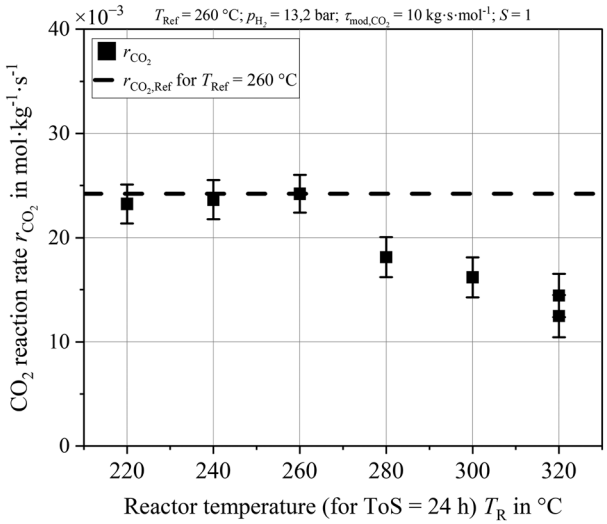

Fig. 4 r_{CO_2} at T_{Ref} = 260 °C after three-phase CO_2 methanation at different T_R for ToS = 24 h; data provided by ref. 38.

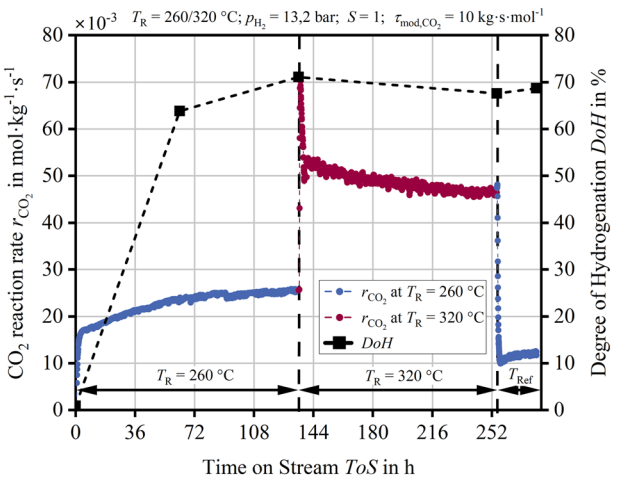

Fig. 5 r_{CO_2} and DoH over ToS for quantification of the loss of catalytic activity for steady-state operation.

Once r_{CO_2} has reached steady state, T_R is reduced again to T_{Ref} = 260 °C. Comparison of $r_{CO_{2,0}}$ before deactivation (ToS ≈ 130 h) with $r_{CO_{2,Ref}}$ after deactivation (ToS ≈ 280 h) shows a decrease of approx. 50%.

Using the experimental procedure presented, the influence of DBT hydrogenation on r_{CO_2} can be neglected, as the DoH is almost constant after ToS = 120 h. The loss of catalytic activity to reach stationary operation is determined to be $r_{CO_{2,Ref}}/r_{CO_{2,0}} \approx 0.5$.

4.3 Identification of the catalyst deactivation mechanism

To identify the mechanism responsible for catalyst deactivation in three-phase CO_2 methanation, the mechanisms discussed in section 2.1 were considered and reaction conditions were adjusted to identify the relevant mechanism.

DBT hydrogenation experiments were performed without CO_2 in the reactor. The experiments are discussed in detail in ref. 36. For these experiments catalyst deactivation was also observed, so the following deactivation mechanisms are ruled out:

- Carbon deposition by Boudouard reaction (eqn (2)) is ruled out, since no CO or CO_2 is present in DBT hydrogenation experiments.
- Catalyst oxidation by water (eqn (4)) is ruled out. In DBT hydrogenation experiments, no water is formed.
- Loss of catalytic activity due to the formation of nickel tetracarbonyls $Ni(CO)_4$ (eqn (3)) is ruled out, since no CO or CO_2 is present in DBT hydrogenation experiments.

Furthermore, catalyst poisoning by impurities in the educt gases is ruled out as a possible deactivation mechanism since deactivation occurs only at high T_R and adsorption of gaseous components should be more pronounced at low temperature.

Catalyst poisoning by impurities in the used isomeric mixture of DBT (Marlotherm SH) was evaluated. Adsorption of impurities on the catalyst surface can be ruled out, as it should be more pronounced at low temperature, whereas catalyst deactivation is observed at high temperature. Another possibility is the decomposition of impurities at high reactor temperature which leads to adsorption of decomposition products. To investigate whether decomposition of impurities is responsible for catalyst deactivation, two experiments, one with fresh and one with reused DBT, were performed.

The CO_2 reaction rate for both experiments is shown in Fig. 6: for the first experiment DBT as it is delivered by the manufacturer was used; for the second experiment DBT from a former experiment was reused. The reused DBT was in the CSTR for at least ToS = 120 h at T_R = 320 °C, therefore it is assumed that a possible decomposition of impurities has occurred and decomposition products are no longer present in the liquid phase. By comparison of the CO_2 reaction rates from these two experiments a possible influence of impurities in DBT can be evaluated. Since reused DBT already exhibits a DoH of approx. 75%, the DoH of fresh DBT was adjusted accordingly by hydrogenation at the beginning of the experiment. This was done by dosing H_2 at T_R = 200 °C for ToS = 72 h. The reused DBT was also hydrogenated for ToS = 24 h to achieve similar DoH for both experiments. Subsequently, CO_2 methanation is started according to the experimental procedure presented in section 3.2.2. The CO_2 reaction rates for both fresh and reused DBT are similar over ToS for the whole experiment at both T_R = 260 °C and T_R = 320 °C. Since no difference in CO_2 reaction rates and extent of catalyst deactivation can be seen for fresh and reused DBT, deactivation is not caused by poisoning due to decomposition of impurities incorporated in commercially available DBT.

Catalyst deactivation is observed at high reactor temperature, whereas DBT adsorption is more pronounced at low temperature. Further, aromatic DBT molecules adsorb

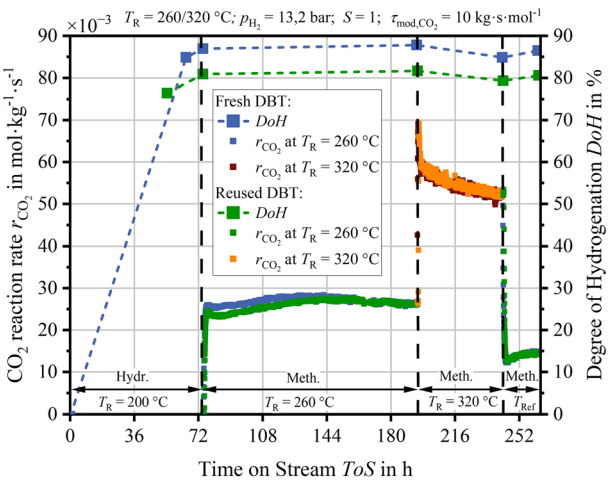

Fig. 6 r_{CO_2} and DoH over ToS for the same reaction conditions using fresh and reused DBT.

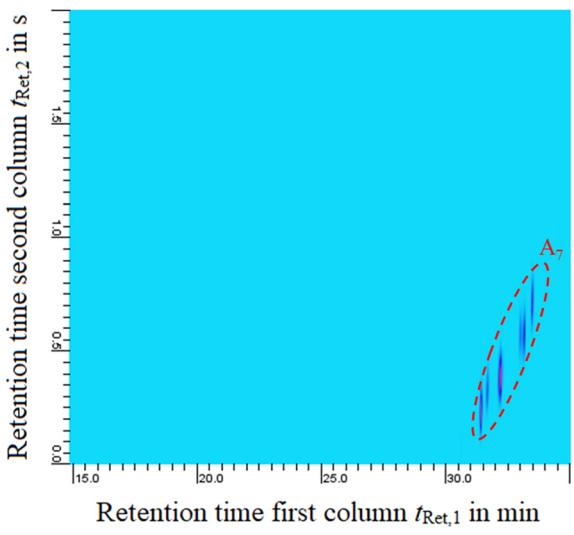

Fig. 7 GC × GC-FID chromatogram of fresh DBT as delivered by the manufacturer.

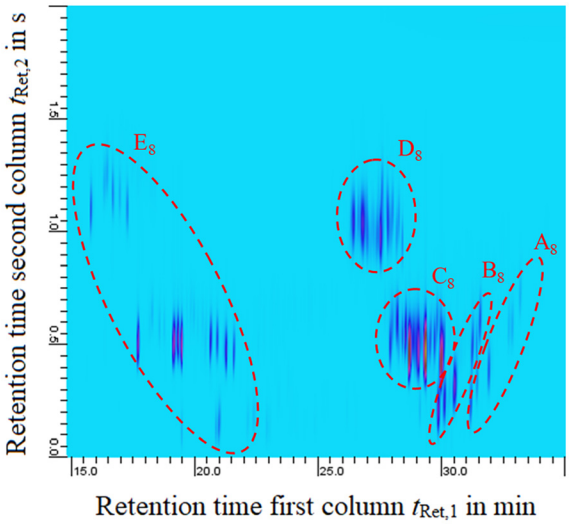

Fig. 8 GC × GC-FID chromatogram of liquid sample taken from the condensate vessel.

stronger on the catalyst surface,[34] so the deactivation should be dependent on the DoH of DBT if it is caused by DBT adsorption. Catalyst deactivation was observed at both low DoH (*e.g.* DoH ≈ 3% at T_R = 320 °C in Fig. 4) and high DoH (*e.g.* DoH ≈ 80% at T_R = 320 °C in Fig. 6). The extent of deactivation is rather dependent on reactor temperature than it is on DoH. Hence, DBT adsorption is ruled out as the cause for the observed catalyst deactivation.

A mechanism dependent on reactor temperature is DBT decomposition, which can lead to catalyst deactivation by adsorption of decomposition products or carbon deposition on the catalyst surface. To check if DBT decomposition occurs, liquid samples of fresh DBT and of evaporated DBT in the condensate vessel were analyzed with GC × GC. The corresponding experiment is shown in Fig. 5; in this case catalyst deactivation was observed. The GC × GC-FID chromatograms of the two samples are shown in Fig. 7 and 8.

In GC × GC analysis two columns are connected in series: in the first column the components are separated regarding their boiling point. Boiling point is increasing with increasing retention time in the first column ($t_{Ret,1}$). Additionally, the components are separated in the second column depending on their polarity. GC × GC analysis was performed in reverse phase setup, and thus the polarity of the components decreases with increasing retention time ($t_{Ret,2}$).

In the fresh DBT sample (Fig. 7) only components with a high retention time in the first column ($t_{Ret,1}$ >30 min) are detected (A_7). Since the fresh DBT sample exhibits a DoH = 0, these are H0-DBT molecules. In the sample taken from the condensate vessel (Fig. 8) the concentration of these molecules is much lower (A_8). This can be explained by their boiling point: these components exhibit high boiling points and tend to remain in the CSTR even at high temperature. Hence, their concentration in the condensate vessel is low.

Another explanation for the low concentration of H0-DBT molecules in the sample taken from the condensate vessel (A_8) is DBT hydrogenation. As discussed in section 2.2, DBT hydrogenation occurs as a side reaction in three-phase CO_2 methanation. A stepwise hydrogenation of the aromatic rings of DBT is observed. As a result, the (partially) hydrogenated DBT components H6-DBT (B_8), H12-DBT (C_8) and H18-DBT (D_8) are detected in the sample taken from the condensate vessel. The polarity and boiling point of partially hydrogenated DBT molecules are decreasing with increasing DoH.

If DBT decomposition occurs in the CSTR, decomposition products with low boiling point should be detected at low $t_{Ret,1}$. These components are observed in the liquid phase sample taken from the condensate vessel, whereas they are not present in the fresh DBT sample. In the chromatogram (see Fig. 8) they are detected at $t_{Ret,1}$ <25 min (E_8). The molecules are identified by mass spectroscopy; they consist of benzyl toluene isomers, xylene, benzene and toluene. These are typical DBT decomposition products which are also observed in DBT dehydrogenation.[28–30] Furthermore, CH_4 was detected in the product gas in DBT hydrogenation experiments. For these experiments no CO_2 is present in the reactor; hence the detected CH_4 also has to be a decomposition product of DBT.

The existence of DBT decomposition products in the condensate vessel and in the gas phase proves that DBT decomposition occurs in three-phase CO_2 methanation with a Ni/SiO_2 catalyst at high reactor temperature. DBT decomposition is a possible cause for the catalyst deactivation observed at high temperature since decomposition occurs at high temperature.

Regarding the possible mechanisms discussed in section 2.1, two are remaining: adsorption of DBT decomposition products and carbon deposition due to DBT decomposition. To check which mechanism is responsible for catalyst deactivation, the fresh reduced catalyst and used deactivated catalyst from the experiment shown in Fig. 5 were analyzed with scanning electron microscopy. The corresponding SEM images are shown in Fig. 9 and 10.

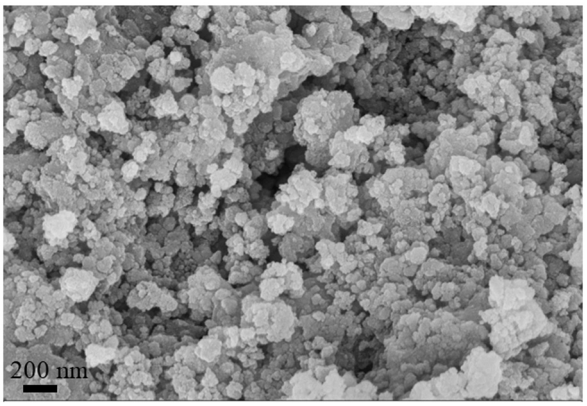

Fig. 9 SEM image of fresh reduced Ni/SiO_2 catalyst.

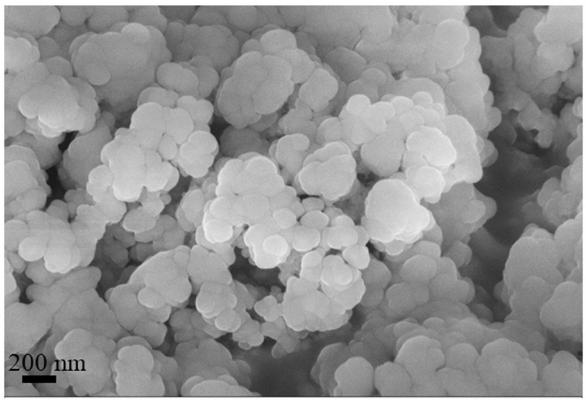

Fig. 10 SEM image of used deactivated Ni/SiO_2 catalyst.

The used deactivated catalyst was prepared for SEM using Soxhlet extraction with toluene to wash off the DBT. Comparing the two SEM images, residues can be seen covering the deactivated catalyst's surface. This could be remaining DBT, which is unlikely due to the vacuum established in SEM. Another explanation is the formation of carbon deposits on the catalyst surface formed by DBT decomposition.

The catalyst was additionally analyzed using TGA. The resulting diagrams are shown in Fig. 11 and 12.

In Fig. 11 the temperature program and the sample mass as a function of time are shown. At the start of the experiment, an inert gas flow of Ar is established and the temperature is increased to 380 °C to allow the evaporation of DBT which is remaining on the catalyst surface. When steady state regarding sample mass is reached, full evaporation of DBT is assumed. The temperature is then increased to 600 °C, resulting in a further loss of sample mass. This loss can be explained by structural changes in the morphology of the catalyst. After steady state is reached, the temperature is decreased to ambient temperature and the gas flow is changed to a mixture of Ar and 3% O_2. In the following temperature ramp up, the sample mass increases

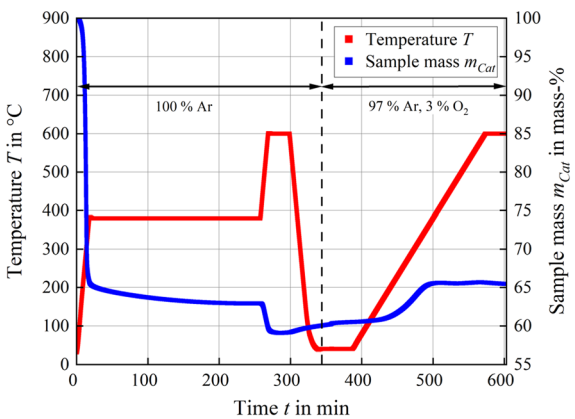

Fig. 11 Temperature program and sample mass of a deactivated Ni catalyst sample wetted by DBT.

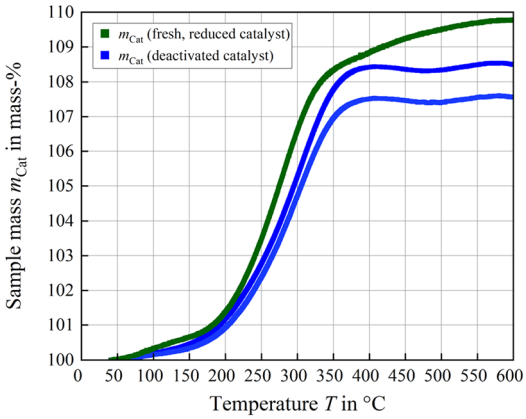

Fig. 12 Excerpt from TGA for the temperature ramp starting at t = 380 min.

due to oxidation of the reduced Ni on the catalyst surface until a temperature of 600 °C is reached.

To check if carbon deposits are present on the deactivated catalyst surface, catalyst samples of fresh reduced catalyst wetted with DBT and of deactivated catalyst wetted with DBT are compared in Fig. 12. The sample mass is shown dependent on temperature for the temperature ramp starting at t ≈380 min of the TGA experiment (Fig. 11). Since the samples differ in the amount of DBT, the remaining sample mass is adjusted to m_{Cat} = 100% after DBT evaporation and structural change in catalyst morphology (t = 380 min).

The mass of both samples is increasing with increasing temperature due to Ni oxidation. Using the nickel loading of the catalyst the theoretical change of catalyst mass by nickel oxidation is calculated to be ≈10%. In the case of the fresh reduced catalyst, this value is reached.

For the deactivated catalyst sample, the sample mass reaches a maximum at around 400 °C. Subsequently, a loss in sample mass is observed, which is possibly due to carbon oxidation and which is not observed for the reduced catalyst sample. As a result of carbon oxidation, new Ni particles are exposed to the O_2 atmosphere, and an increase in sample mass follows. These steps are repeated, so an alternating sample mass is detected. This phenomenon is not observed for the fresh reduced catalyst.

In summary, thermogavimetric analysis of the deactivated catalyst shows a reduction in sample mass at high temperature in an O_2-containing atmosphere. This is probably due to the oxidation of carbon deposits formed on the catalyst surface by DBT decomposition.

Conclusions

In this work, catalyst deactivation in three-phase CO_2 methanation was observed. An experimental procedure was chosen to eliminate the influence of DBT hydrogenation reaction on CO_2 methanation reaction rate to quantify the loss in catalytic activity.

Catalyst deactivation is observed for T_R >260 °C; the loss in catalytic activity increases with increasing T_R. Experiments at high T_R showed that the loss in catalytic activity for steady-state operation is approx. 50%.

Reaction conditions were varied to investigate the mechanism responsible for catalyst deactivation. Product gas analysis and liquid phase analysis by GC × GC showed that DBT decomposition is occurring in three-phase CO_2 methanation at high temperature. Analysis of the used catalyst showed that catalyst deactivation is caused by carbon deposition on the catalyst surface.

The catalyst deactivation mechanism presented in this work should be considered regarding reactor design and operating conditions chosen for three-phase CO_2 methanation in a slurry bubble column reactor. Further, the observation of catalyst deactivation due to DBT decomposition and carbon deposition is also of interest for other applications such as the use of DBT as a liquid organic hydrogen carrier.

Author contributions

M. Held: methodology, conceptualization, investigation, data curation, writing – original draft, writing – review & editing. A. Holfelder: investigation, data curation. S. Bajohr: writing – review & editing, funding acquisition. T. Kolb: writing – review & editing, supervision.

Conflicts of interest

The authors declare that there are no conflicts of interest.

Data availability

All data supporting the findings in this article have been included in the figures and main manuscript. Further inquiries can be directed to the corresponding author.

Acknowledgements

This project was financially supported by the Federal Ministry of Education and Research in the scope of the project InnoSyn. Further, we thank Jonathan Rummel and Prof. Reinhard Rauch from Engler-Bunte-Institut, Fuel Technology for execution and analysis of the GC × GC measurements presented in this work.

References

1 M. Wietschel, S. Ullrich, P. Markewitz, F. Schulte and F. Genoese, *Energietechnologien der Zukunft*, Springer, 2015.
2 M. Zapf, *Stromspeicher und Power-to-Gas im deutschen Energiesystem*, Springer, 2017.
3 A. Varone and M. Ferrari, *Renewable Sustainable Energy Rev.*, 2015, **45**, 207–218.
4 J. Kopyscinski, T. J. Schildhauer and S. M. A. Biollaz, *Fuel*, 2010, **89**, 1763–1783.
5 S. Matthischke, S. Roensch and R. Guttel, *Ind. Eng. Chem. Res.*, 2018, **57**, 6391–6400.
6 R. T. Zimmermann, J. Bremer and K. Sundmacher, *Chem. Eng. J.*, 2020, **387**, 123704.
7 P. Strucks, L. Failing and S. Kaluza, *Chem. Ing. Tech.*, 2021, **93**, 1526–1536.
8 M. Held, D. Schollenberger, S. Sauerschell, S. Bajohr and T. Kolb, *Chem. Ing. Tech.*, 2020, **92**, 595–602.
9 S. Sauerschell, S. Bajohr and T. Kolb, *Energy Fuels*, 2022, **36**, 7166–7176.
10 J. Lefebvre, S. Bajohr and T. Kolb, *Fuel*, 2019, **239**, 896–904.
11 P. Sabatier, *C. R. Hebd. Seances Acad. Sci.*, 1902, **134**, 514–516.
12 S. Kattel, P. Liu and J. G. Chen, *J. Am. Chem. Soc.*, 2017, **139**, 9739–9754.
13 G. A. Mills and F. W. Steffgen, *Catal. Rev.:Sci. Eng.*, 1974, **8**, 159–210.
14 S. Rönsch, J. Schneider, S. Matthischke, M. Schlüter, M. Götz, J. Lefebvre, P. Prabhakaran and S. Bajohr, *Fuel*, 2016, **166**, 276–296.
15 M. Götz, J. Lefebvre, F. Mörs, A. M. Koch, F. Graf, S. Bajohr, R. Reimert and T. Kolb, *Renewable Energy*, 2016, **85**, 1371–1390.
16 T. Schaaf, J. Grünig, M. R. Schuster, T. Rothenfluh and A. Orth, *Energy Sustain. Soc.*, 2014, **4**, 2.
17 B. Miao, S. S. K. Ma, X. Wang, H. Su and S. H. Chan, *Catal. Sci. Technol.*, 2016, **6**, 4048–4058.
18 S. Ewald, M. Kolbeck, T. Kratky, M. Wolf and O. Hinrichsen, *Appl. Catal., A*, 2019, **570**, 376–386.
19 C. H. Bartholomew, *Appl. Catal., A*, 2001, **212**, 17–60.
20 J. R. Rostrup-Nielsen, K. Pedersen and J. Sehested, *Appl. Catal., A*, 2007, **330**, 134–138.
21 M. S. Spencer, *Nature*, 1986, **323**, 685–687.
22 M. Götz, *PhD thesis*, Karlsruher Institut für Technologie (KIT), 2014.
23 M. Seemann, *PhD thesis*, ETH Zurich, 2007.
24 P. K. Agrawal, W. D. Fitzharris and J. R. Katzer, *Studies in Surface Science and Catalysis: Catalyst Deactivation*, Elsevier, 1980, vol. 6, pp. 179–200.
25 C. H. Bartholomew, *Catal. Rev.:Sci. Eng.*, 1982, **24**, 67–112.
26 J. Kopyscinski, T. J. Schildhauer and S. M. Biollaz, *Chem. Eng. Sci.*, 2011, **66**, 924–934.
27 S. E. Olesen, K. J. Andersson, C. D. Damsgaard and I. Chorkendorff, *J. Phys. Chem. C*, 2017, **121**, 15556–15564.
28 P. Modisha, P. Gqogqa, R. Garidzirai, C. N. M. Ouma and D. Bessarabov, *Int. J. Hydrogen Energy*, 2019, **44**, 21926–21935.
29 P. Modisha, R. Garidzirai, H. Güneş, S. E. Bozbag, S. Rommel, E. Uzunlar, M. Aindow, C. Erkey and D. Bessarabov, *Catalysts*, 2022, **12**, 489.
30 M. Xu, R. Gao, C. Shi, Z.-F. Huang, X. Zhang, J.-J. Zou and L. Pan, *Chem. Eng. Sci.*, 2024, **287**, 119754.
31 W. M. Shen, J. A. Dumesic and C. G. Hill Jr, *J. Catal.*, 1981, **68**, 152–165.
32 H. Harms, B. Höhlein and A. Skov, *Chem. Ing. Tech.*, 1980, **52**, 504–515.

33 R. P. Struis, T. J. Schildhauer, I. Czekaj, M. Janousch, S. M. A. Biollaz and C. Ludwig, *Appl. Catal., A*, 2009, **362**, 121–128.
34 A. Leinweber, *PhD thesis*, Universität Rostock, 2022.
35 N. E. Tsakoumis, M. Rønning, Ø. Borg, E. Rytter and A. Holmen, *Catal. Today*, 2010, **154**, 162–182.
36 M. Held, A. Rieck, S. Bajohr and T. Kolb, *Int. J. Hydrogen Energy*, 2025, **132**, 166–173.
37 J. Lefebvre, N. Trudel, S. Bajohr and T. Kolb, *Fuel*, 2018, **217**, 151–159.
38 A. L. Rieck, *Master's Thesis*, Karlsruhe Institute of Technology, Karlsruhe, 2024.